Acta Cryst. (1970). A**26**, 263

Neutron Diffraction Study of the Atomic and Molecular Motion in Hexamethylenetetramine

BY J. A. K. DUCKWORTH AND B. T. M. WILLIS
Atomic Energy Research Establishment, Harwell, Berkshire, England

AND G. S. PAWLEY
Department of Natural Philosophy, Edinburgh University, Scotland

(*Received* 16 *July* 1969)

An accurate neutron diffraction study has been carried out on a single crystal of hexamethylenetetramine and the measured Bragg intensities have been analysed for the effects of thermal motion. Four different models of the thermal motion have been used in a least-squares refinement of the data: (1) conventional model with ellipsoidal atomic probability density functions; (2) cumulant expansion model with the thermal motion of each atom represented by both second and third cumulant coefficients; (3) as model (1) but including the restriction imposed on the temperature factors by assuming rigid-body molecular motion; (4) as model (2) but including the rigid-body restriction. The best fit is given by model (2), which takes into account deviations from the ellipsoidal atomic probability density functions brought about by libration. Of the rigid-body models, refinement is better for (4) than for (3). Two parameters only, $\langle u^2 \rangle$ and $\langle \omega^2 \rangle$ of paper I (Willis & Pawley, *Acta Cryst.* (1970), A**26**, 254) are needed to specify the atomic thermal motions for models (3) and (4), whereas nine parameters are required for model (1) and twenty for model (2). The lone-pair electrons of the nitrogen atom have been detected by combining, in a difference Fourier synthesis, the present data with the X-ray measurements of Becka & Cruickshank (*Proc. Roy. Soc.* A (1963), **273**, 435).

1. Introduction

We report in this paper the results of a study, by neutron diffraction, of a single crystal of hexamethylenetetramine, HMT. Appreciable care was taken to obtain accurate measurements of the Bragg intensities, which have been analysed to yield parameters describing the atomic and molecular thermal motion. HMT was chosen for this work because it possesses exceptionally high crystal and molecular symmetry, thus reducing the number of independent parameters required for the various models of the thermal motion. The experiment was carried out with neutrons, as the hydrogen atoms in the molecule of HMT, of formula $C_6N_4H_{12}$, undergo the largest amplitudes of vibration.

X-ray (Brill, Grimm, Hermann & Peters, 1939), electron (Lobatchev, 1954) and neutron (Andresen, 1957) studies of HMT have established the coordinates of the atoms in this molecular crystal. The space group is cubic, $I\bar{4}3m$, which utilizes the full cubic point symmetry, $\bar{4}3m$, of the molecule (see Fig. 1). In a careful X-ray investigation by Becka & Cruickshank (1963), the anisotropic atomic-vibration amplitudes were analysed to give the rigid-body translational and librational amplitudes of the molecule, using the first-order rigid-body theory described in § 2.3(*b*) of paper I. We shall show that the present neutron data refine more satisfactorily using the second-order rigid-body treatment given in § 2.3(*c*) of paper I, but that a better fit still is obtained with the cumulant-expansion model (Johnson, 1969), which allocates individual atomic cumulant coefficients to represent the thermal motion.

We discuss also small differences between the atomic coordinates derived from the present neutron study and those obtained from the X-ray study of Becka & Cruickshank. These differences can be ascribed to the influence of lone-pair and bonding electrons associated with the nitrogen and hydrogen atoms respectively.

2. Experimental

Intensity data from a single crystal were collected on a Hilger and Watts automatic neutron diffractometer, using the moving-crystal, moving-detector technique ($\omega/2\theta$ scan) with a neutron wavelength of 1·038 Å. 49 independent F values were measured up to $\sin\theta/\lambda = 0{\cdot}80$ at a temperature of 20 °C.

The following steps were taken to improve the precision of the measurements.

2.1 *Beam uniformity*

The uniformity in intensity of the beam reflected by the crystal monochromator was determined by scanning across the beam with a small pinhole of cadmium. The variation of intensity was ± 3 % over a circle 5 mm in diameter: the HMT crystal was positioned to lie at the centre of this circle.

2.2 *Symmetry-related measurements*

HMT crystallizes in the cubic system, so that there are up to 24 symmetry-related Friedel pairs for each Bragg reflexion. Each measured structure factor was obtained by averaging over n observations (see Table 1), one from each of n Friedel pairs taken from the set

$\{h_1\ h_2\ h_3\}$, and an estimate of the standard error σ of the structure factor was obtained from the variance of the n observations.

2.3 *Double-Bragg scattering*

Double-Bragg scattering gives rise to an intensity error which is extremely difficult to correct for (Arndt & Willis, 1966). However, the magnitude of the error is very sensitive to the angle of rotation ψ about the diffraction vector.

In the present experiment ψ was incremented by 2° before each intensity measurement was made. Thus the quantity σ, which reflects the spread in the magnitudes of the n measurements for a symmetry-related set, must include a contribution from double-Bragg effects.

2.4 *Counting statistics*

The counting time for each measurement was sufficient to ensure a statistical uncertainty in the recorded intensity of less than 2% for most reflexions.

3. Processing of diffraction data

Corrections were made for absorption, thermal diffuse scattering, and extinction, as follows.

3.1 *Absorption*

The linear absorption coefficient μ was measured directly as 3·02 cm^{-1}. The 'absorption' arises almost entirely from incoherent spin scattering by hydrogen; the observed μ value corresponds to an effective incoherent scattering cross-section of 36 barns per hydrogen atom.

To calculate the transmission factor A^*, the crystal was taken to be spherical with an effective radius of 1·3 mm. A^* was obtained from new absorption tables for a sphere with numbers correct to 1 part in 10^3 (Rouse, 1969).

3.2 *Thermal diffuse scattering*

As in the case of X-ray scattering, the thermal diffuse scattering of neutrons close to the Bragg peak can give rise to an appreciable error in the estimated Bragg intensity. The TDS correction for neutrons can be calculated by the same theory as for X-rays, provided the neutron velocity exceeds the velocity of sound in the crystal (Willis, 1969).

The elastic constants of HMT are (Haussühl, 1958)

$$c_{11}=1{\cdot}643.\quad 10^{11}\ \text{erg.cm}^{-3}$$
$$c_{12}=0{\cdot}433.\quad 10^{11}\ \text{erg.cm}^{-3}$$
$$c_{44}=0{\cdot}515.\quad 10^{11}\ \text{erg.cm}^{-3}.$$

The condition for elastic isotropy ($c_{11}-c_{12}=2c_{44}$) is nearly satisfied, so that the two transverse acoustic modes propagate with almost the same velocity

$$(c_{44}/\varrho)^{1/2}=1{\cdot}96.\quad 10^5\ \text{cm.sec}^{-1}$$

and the longitudinal mode with the velocity

$$(c_{11}/\varrho)^{1/2}=3{\cdot}50.\quad 10^5\ \text{cm.sec}^{-1},$$

where the density $\varrho=1{\cdot}339\ \text{g.cm}^{-3}$. The velocity of 1·038 Å neutrons is 3·82. 10^5 cm.sec^{-1}, which exceeds the velocities of both types of acoustic wave. Thus we

Table 1. *Neutron structure factor data for HMT*
F values are on a relative scale only.

h_1	h_2	h_3	n	F_{obs}^{uncorr}	σ_s	$\sigma(F_{obs}^{uncorr})$	$/A^*$	$\sqrt{1+\alpha}$	F_{obs}	$\sigma(F_{obs})$
1	1	0	6	5.493	0.010	0.070	1.338	1.0009	10.714	0.140
2	0	0	18	2.250	0.007	0.015	1.338	1.0023	3.154	0.021
2	1	1	15	4.702	0.006	0.048	1.338	1.0040	7.448	0.079
2	2	0	18	2.243	0.009	0.015	1.338	1.0058	3.089	0.021
3	1	0	24	3.454	0.006	0.019	1.334	1.0077	4.922	0.027
2	2	2	9	6.025	0.012	0.070	1.334	1.0097	9.720	0.114
3	2	1	12	4.929	0.010	0.029	1.334	1.0118	7.370	0.045
4	0	0	12	3.105	0.012	0.020	1.334	1.0140	4.283	0.028
3	3	0	12	3.559	0.010	0.025	1.334	1.0162	4.954	0.035
4	1	1	14	2.216	0.012	0.017	1.334	1.0162	2.976	0.023
4	2	0	11	2.181	0.014	0.020	1.334	1.0185	2.916	0.028
3	3	2	14	2.496	0.012	0.023	1.334	1.0208	3.349	0.032
4	2	2	12	1.482	0.020	0.020	1.334	1.0231	1.949	0.029
4	3	1	12	4.921	0.013	0.030	1.334	1.0255	7.029	0.043
5	1	0	10	1.289	0.027	0.011	1.334	1.0255	1.687	0.014
5	2	1	12	2.641	0.015	0.016	1.330	1.0303	3.496	0.021
4	4	0	12	7.585	0.012	0.043	1.330	1.0327	11.888	0.068
5	3	0	15	4.562	0.013	0.020	1.330	1.0351	6.291	0.028
4	3	3	11	1.405	0.028	0.030	1.330	1.0351	1.818	0.039
4	4	2	13	1.998	0.019	0.024	1.330	1.0376	2.569	0.031
5	3	2	15	3.110	0.013	0.026	1.330	1.0400	4.103	0.034
6	1	1	12	3.994	0.012	0.019	1.330	1.0400	5.378	0.025
6	2	0	12	2.196	0.019	0.029	1.330	1.0424	2.845	0.038
5	4	1	12	3.436	0.015	0.017	1.330	1.0449	4.536	0.023
6	2	2	12	5.303	0.015	0.020	1.330	1.0474	7.328	0.029
6	3	1	12	2.332	0.018	0.027	1.330	1.0498	3.002	0.034
7	1	0	12	2.024	0.022	0.025	1.330	1.0546	2.583	0.032
5	5	0	6	2.184	0.029	0.032	1.330	1.0546	2.792	0.041
5	4	3	12	1.389	0.030	0.041	1.330	1.0546	1.762	0.052
6	3	3	12	2.644	0.018	0.030	1.330	1.0594	3.384	0.039
7	2	1	11	1.936	0.024	0.020	1.330	1.0594	2.456	0.025
7	3	2	12	1.710	0.026	0.027	1.326	1.0689	2.137	0.034
6	5	1	12	1.237	0.034	0.027	1.326	1.0689	1.541	0.034
8	0	0	6	5.408	0.021	0.039	1.326	1.0712	7.216	0.052
8	1	1	12	3.019	0.017	0.020	1.326	1.0735	3.817	0.026
8	2	0	11	1.668	0.028	0.030	1.325	1.0758	2.068	0.037
6	5	3	11	1.981	0.024	0.026	1.323	1.0785	2.454	0.032
6	6	2	12	3.094	0.017	0.018	1.323	1.0846	3.862	0.023
7	5	2	12	1.878	0.024	0.027	1.323	1.0867	2.305	0.033
9	1	0	12	1.749	0.026	0.027	1.323	1.0909	2.136	0.033
8	3	3	12	1.346	0.032	0.020	1.323	1.0909	1.639	0.034
7	6	1	12	1.774	0.026	0.020	1.319	1.0949	2.153	0.024
7	5	4	12	1.310	0.033	0.028	1.319	1.0989	1.596	0.046
8	4	4	10	3.167	0.017	0.023	1.319	1.1044	3.871	0.028
8	5	3	12	1.783	0.025	0.043	1.319	1.1061	2.142	0.051
4	3	9	12	1.718	0.025	0.023	1.315	1.1126	2.044	0.027
2	2	10	12	1.816	0.023	0.015	1.315	1.1140	2.160	0.018
6	6	6	4	1.846	0.040	0.039	1.315	1.1140	2.196	0.046
5	5	8	12	1.260	0.032	0.026	1.314	1.1181	1.485	0.030

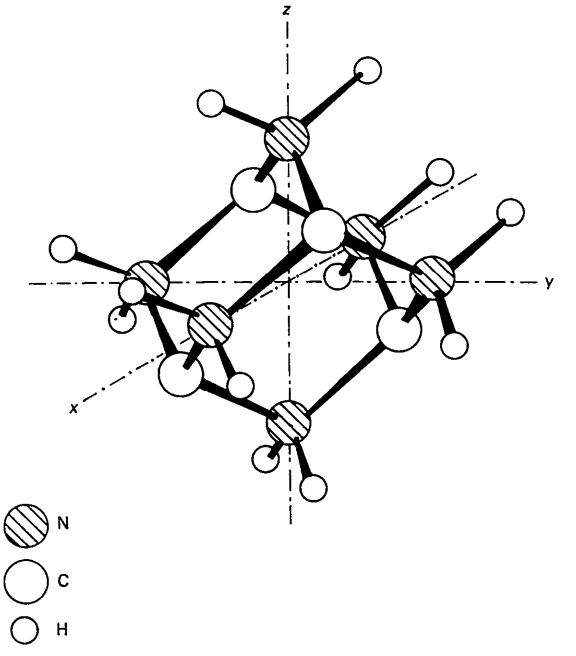

Fig. 1. Molecule of HMT with cubic axes shown as chain-dotted lines.

can apply the same kind of TDS correction as for X-ray scattering.

The TDS correction α to the observed intensity I_{obs} is defined by

$$I_{obs} = I_{Bragg}\,(1+\alpha)$$

where I_{Bragg} is the required intensity contributed by elastic scattering alone. The procedure described by Cooper & Rouse (1968) was used to calculate α for each reflexion: the input parameters for this calculation were the elastic constants, the scanning range in ω (2·0°), and the angles subtended by the detector at the crystal (3·8° in the horizontal plane and 5·4° in the vertical plane).

3.3 *Extinction*

In the initial stages of the data analysis it was evident that the strongest reflexions were affected appreciably by extinction. The complete set of data was corrected for extinction using the theory of Zachariasen (1967).

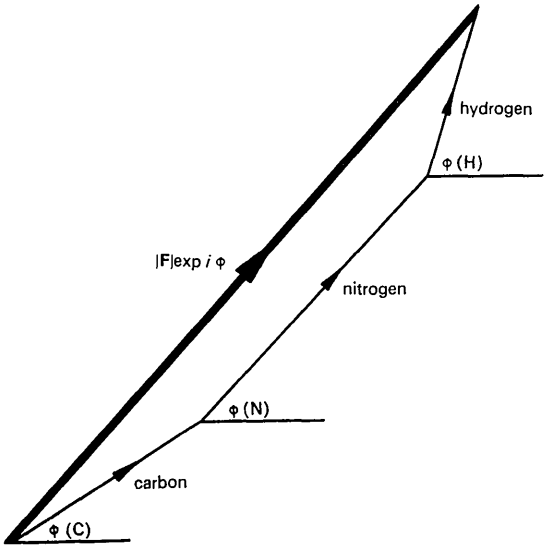

Fig. 2. Vector representation of a structure factor, showing contributions from carbon, nitrogen and hydrogen.

For a spherical crystal the extinction equations of Zachariasen reduce to the following form:

$$F_{obs}^{uncorr} = F_{obs}^{corr}\, y^{1/2} \qquad (1a)$$

$$y = y^* = (1+x^{*2})^{1/2} - x^* \qquad (1b)$$

$$x^* = c\,(F_{obs}^{uncorr})^2 \operatorname{cosec} 2\theta\,. \qquad (1c)$$

y is the reduction in intensity due to extinction and F_{obs}^{corr} is the structure factor corrected for extinction. c is a constant which is determined by the degree of extinction in the crystal and is the same for all reflexions. Once c is known, equation (1) can be used to convert each F_{obs}^{uncorr} to F_{obs}^{corr}.

c was determined in the following way. By omitting the strongest reflexions, first estimates of the atomic coordinates and temperature factors were derived from a conventional least-squares refinement (with individual atomic temperature factors). These estimates were used to calculate the structure factors F_{calc} of the omitted reflexions, and by putting $F_{calc} = F_{obs}^{corr}$ in equation (1a) the quantity y was obtained for these reflexions. x^* could then be calculated from (1b) and a first estimate of c from (1c) by plotting x^* *versus* $(F_{obs}^{uncorr})^2$ cosec 2θ. Using this value of c, y was calculated for all reflexions, and by employing the corrected structure factors $F_{obs}^{uncorr}\, y^{-1/2}$, revised estimates of the atomic coordinates and temperature factors were obtained. c converged to a constant value after three iterations.

The value of c in equation (1c) found in this way was 0·00343, in units appropriate to the results of Table 1. At a later stage in the refinement the value of c was introduced as a variable least-squares parameter. A very small change was indicated, giving the final value of c as $0{\cdot}00321 \pm 0{\cdot}0004$. This is the value used to obtain the corrected values in Table 1. The strongest reflexion *110* was reduced in intensity by 55% from extinction.

3.4 *Final listing of structure factors*

Column 2 in Table 1 gives n, the number of symmetry-related measurements made for each family of planes $h_1h_2h_3$. Column 3 contains the magnitudes of the uncorrected structure factors, obtained by averaging

Table 2. *Symmetry relations for second and third cumulants*

Numbers in parentheses are multiplicities.

Second cumulants

Atom	b_{11}	b_{22}	b_{33}	b_{23}	b_{31}	b_{12}
	(1)	(1)	(1)	(2)	(2)	(2)
Carbon	b_{11}	b_{22}	b_{22}	b_{23}	0	0
Nitrogen	b_{11}	b_{11}	b_{11}	b_{23}	b_{23}	b_{23}
Hydrogen	b_{11}	b_{11}	b_{33}	b_{23}	b_{23}	b_{12}

Third cumulants

Atom	c_{111}	c_{222}	c_{333}	c_{112}	c_{122}	c_{113}	c_{133}	c_{223}	c_{233}	c_{123}
	(1)	(1)	(1)	(3)	(3)	(3)	(3)	(3)	(3)	(6)
Carbon	c_{111}	0	0	0	c_{122}	0	c_{122}	0	0	c_{123}
Nitrogen	c_{111}	c_{111}	c_{111}	c_{112}	c_{112}	c_{112}	c_{112}	c_{112}	c_{112}	c_{123}
Hydrogen	c_{111}	c_{111}	c_{333}	c_{112}	c_{112}	c_{113}	c_{133}	c_{113}	c_{133}	c_{123}

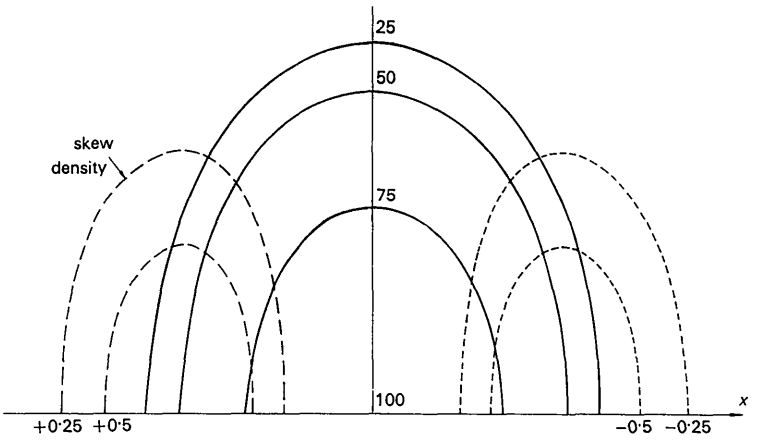

Fig. 3. Edgeworth map (probability density function) for the carbon atom – full lines. The skew density map is superimposed – broken lines. The Edgeworth map is normalized to 100 at the atom site, and is symmetrical about the x axis: the skew map is on the same scale.

over these n measurements. σ_s in column 4 is the standard deviation given by counting statistics alone, and $\sigma(F^{\text{uncorr}})$ in column 5 is the standard error calculated from the variance of the n measurements. Columns 6 and 7 list the structure-factor corrections arising from absorption and TDS. After applying these corrections and the extinction correction, the final values of F_{obs} and $\sigma(F_{\text{obs}})$ in the last two columns are obtained. Reflexions in the range $0 < \sin\theta/\lambda < 0{\cdot}8$ which are missing from Table 1 are very weak or unobservable.

The estimated contribution to the R index due to uncertainties in the F_{obs}'s is (Arndt & Willis, 1966)

$$0{\cdot}7979\ \Sigma\ \sigma(F_{\text{obs}})/\ \Sigma\ F_{\text{obs}}$$

which is 0·80% for the figures in Table 1.

4. Refinement using the cumulant-expansion model

A least-squares program was written to minimize the quantity

$$\sum_{h_1h_2h_3} w(F_{\text{obs}}^{\text{corr}} - s\,|F_{\text{calc}}|)^2 \qquad (2)$$

where w is $1/\sigma^2$, s is an overall scale factor and F_{calc} is given by the cumulant-expansion model of Johnson (1970):

$$F_{\text{calc}} = \sum_{\kappa} b_\kappa \exp(2_i^\kappa \pi i x h_i) \exp(-b_{ij}^\kappa h_i h_j) \exp(-ic_{ijk}^\kappa h_i h_j h_k) \exp(d_{ijkl}^\kappa h_i h_j h_k h_l)\,. \qquad (3)$$

The refinable parameters were s and, for each atom (κ), b, x_i, b_{ij}, c_{ijk} and d_{ijkl} ($i, j, k, l = 1, 2, 3$). These atomic parameters are zero-, first- ... fourth-rank tensors, respectively, and the double-summation convention is assumed in equation (3).

(a) *Conventional refinement*

In the conventional refinement procedure, the second cumulants, b_{ij}, are the anisotropic temperature factors, and the third cumulants, c_{ijk}, and fourth cumulants, d_{ijkl}, are set to zero. The three atoms of the asymmetric unit are in the following special positions: carbon at $u'\ 0\ 0$ with site symmetry $2mm$, nitrogen at $v\ v\ v$ with site symmetry $3m$, hydrogen at $x\ x\ z$ with site symmetry m. These site symmetries lead to the symmetry relations between the second-cumulant coefficients listed in Table 2. Thus for the conventional model we need to determine 1 scale factor, 4 first-cumulant coefficients and 9 second-cumulant coefficients, assuming that the scattering lengths b_κ are fixed (0·663, 0·940, and $-0{\cdot}374\ 10^{-12}$ cm for C, N, and H respectively). The 14 parameters from this refinement, corresponding to an R index of 2·33%, are given in column 1 of Table 3.

Table 3. *Parameters determined by various refinement procedures described in the text.*

	Conventional (second cumulants only)	Second and third cumulants	Second-order rigid-body model
Carbon			
u'	0·2370 (5)*	0·2356 (8)*	
b_{11}	0·0103 (6)	0·0101 (6)	0·0108
b_{22}	0·0259 (6)	0·0254 (6)	0·0265
b_{23}	0·0001 (10)	−0·0001 (8)	0
c_{111}	–	−0·00032 (14)	0
c_{122}	–	−0·00016 (10)	−0·00012
c_{123}	–	0	0
Nitrogen			
v	0·1222 (2)*	0·1225 (4)*	
b_{11}	0·0196 (3)	0·0197 (3)	0·0191
b_{12}	−0·0041 (3)	−0·0041 (3)	−0·0042
c_{111}	–	0·00008 (16)	−0·00010
c_{112}	–	−0·00001 (10)	0
c_{123}	–	−0·00002 (16)	0·00005
Hydrogen			
x	0·0909 (6)*	0·0904 (8)*	
z	−0·3266 (7)*	−0·3229 (12)*	
b_{11}	0·0444 (14)	0·0435 (12)	0·0438
b_{33}	0·0206 (11)	0·0233 (12)	0·0157
b_{12}	−0·0021 (16)	−0·0026 (12)	−0·0023
b_{13}	0·0095 (8)	0·0101 (7)	0·0084
c_{111}	–	−0·00048 (27)	−0·00029
c_{333}	–	0·00073 (26)	0·00015
c_{112}	–	−0·00000 (16)	−0·00008

Table 3 (*cont.*)

c_{113}	–	0·00063 (20)	0·00030
c_{133}	–	0·00041 (16)	0·00016
c_{123}	–	0·00013 (18)	−0·00007
R	2·33%	1·18%	

* Uncorrected for libration.

(*b*) *Higher-cumulants refinement*

For the third-cumulant refinement, there are 12 additional parameters representing the symmetry-independent third-cumulant coefficients (see Table 2). All 12 parameters were varied in the first attempt at refinement, but three parameters, c_{123} (C), c_{123} (N) and c_{123} (H), were found to have unit correlations. The inter-dependence of these three parameters arises for the following reason. The structure factor of the $h_1h_2h_3$ reflexion is a sum over the individual atom contributions, where each contribution contains phase factors $\exp(-ic^{\kappa}_{123}h_1h_2h_3)$ from the third cumulant. Consider the set of coefficients c_{123} for one atom type; these coefficients are unchanged by the symmetry operations relating equivalent atomic positions, and this allows the phase factors above to be factorized. Thus there are three phase factors, say $\exp i\varphi$(C), $\exp i\varphi$(N) and $\exp i\varphi$(H) from the three atom types, and the structure factor can be represented vectorially as the sum of contributions from the three atom types. This is shown in Fig. 2, where the structure factor is $|F|\exp i\varphi$. φ is evidently arbitrary, and so only two of the three phase factors are independent.

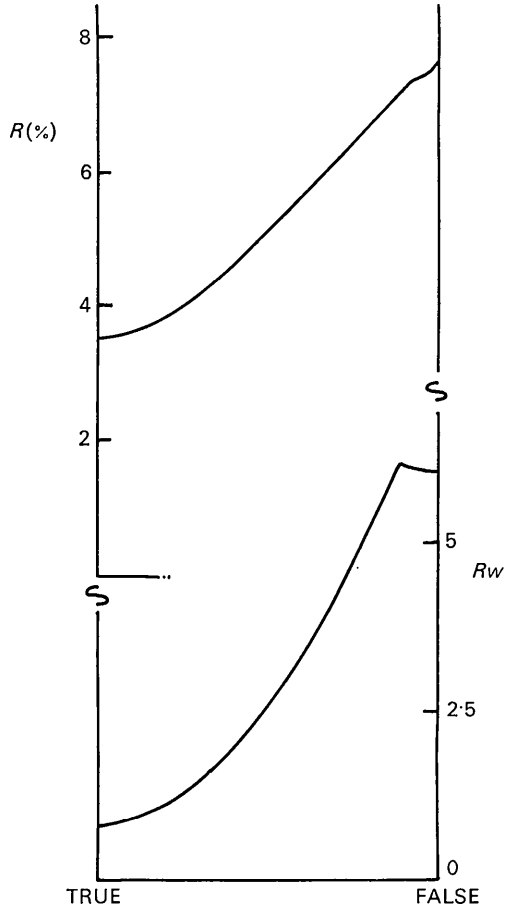

Fig. 4. The variation of R_w and of R between the false and the true least-squares minima.

In a second attempt at a third-cumulant refinement, c_{123} (C) was set to zero. Refinement now proceeded satisfactorily and after two cycles of refinement the R index converged to 1·18%, which is close to the limit set by the accuracy of the observations. Table 3, column 2, lists the 25 parameters derived from this analysis.

For the fourth-cumulant refinement [*i.e.* using the complete expression (3)] the number of variable parameters increases to 44. As the total number of independent observations was only 49, the results from this refinement (leading to $R=1{\cdot}14\%$) will not be quoted. Moreover, according to the rigid-body analysis of paper I (discussed in § 5 below), the fourth cumulants vanish – but not the third cumulants – if terms of higher order than $\langle\omega^2\rangle^2$ are neglected.

An Edgeworth map (Johnson, 1970) which is the representation of the probability density function (p.d.f.) of an atom, was plotted for the three types of atom using the parameters in Table 3 for the third-cumulant refinement. The map for carbon is illustrated in Fig. 3: the small asymmetry of the p.d.f. is due to libration, which is more readily seen on the skew map (Johnson, 1970) represented by the broken lines on the same Figure.

5. Refinement using the rigid-body model

In the rigid-body model, two parameters only, $\langle u^2\rangle$ and $\langle\omega^2\rangle$ of paper I, are needed to specify the effect of thermal motion, whereas nine independent parameters (b^{κ}_{ii}) are required for the second-cumulant model and twenty (b^{κ}_{ii} and c^{κ}_{ijk}) for the third-cumulant model. Equation (3.2) of paper I gives the calculated structure factor correct to $\langle\omega^2\rangle^2$, in terms of $\langle u^2\rangle$ and $\langle\omega^2\rangle$. This equation was used in writing a second least-squares program to minimize the expression (2).

(*a*) *First-order rigid-body refinement*

In the first-order treatment, terms in $\langle\omega^2\rangle^2$ are neglected [see § 2.3(*b*) of paper I]. The refined values of the seven variable parameters (excluding the scale fac-

Table 4. *Parameters from the rigid-body analysis*

	First order		Second order	Units
	True	False		
u'	0·2359	0·2426	0·2356	Fractional
v	0·1216	0·1177	0·1214	
x	0·0910	0·0894	0·0906	
z	−0·3279	−0·3359	−0·3270	
$\langle u^2\rangle$	0·0271	0·0262	0·0263	Å²
$\langle\omega^2\rangle$	47·7	53·9	49·0	deg²
R	3·23	7·7	3·02	%

tor) are listed in column 1 of Table 4. The R index was 3·23% which is appreciably higher than the R index of 2·33% for the corresponding refinement without the rigid-body constraint [§ 4(*a*)]. To the authors' knowledge this is the first time in which the rigid-body constraint applied to a molecular crystal has given a less satisfactory refinement than the unconstrained procedure.

In carrying out the first-order refinement a false minimum was discovered with an R index of 7·7%. The parameters of the false minimum are given in Table 4, column 2. The origin of this false minimum was traced as follows.

The structure factor of each reflexion varies between the two points in parameter space defined by the parameters for the true and false minima. Taking a straight line in parameter space with these two points as end points and dividing the line into ten equal parts, the structure factors were calculated at these intervals. Of the 49 values of $F_{\rm calc}$, 45 varied monotonically and the remaining 4 varied in the way indicated in Table 5.

The variation in three of these reflexions is small and cannot be the cause of the false minimum: we conclude that the 510 reflexion is the sole cause. The sign of 510 changed near the false minimum, giving a similar but more dramatic effect to that noted in adamantane by Donohue & Goodman (1967). These authors found that two reflexions caused a false minimum.

Fig. 4 shows the variation of the R index and the weighted sum of deviations R_w along the line between the two minima. There is a turning point in R_w but not in R, so that a refinement minimizing R rather than the customary R_w would not encounter the false minimum. It is generally recognized that a refinement on R can be started further from the correct position in parameter space than is possible by the usual least-squares refinement on R_w. This arises from the smoother variation of R in parameter space and suggests mixing of both refinement procedures to avoid false minima.

Why is the 510 sign change of such importance? In Fig. 5 arrows join the atomic positions for the false and the true minima. The solid lines are the zeros of

$$\cos 2\pi\,(5x+y)$$

and are the lines across which the cosine varies most rapidly. All atoms except the carbon atoms lie near these lines (or symmetry-related lines) and so we would expect $F_{\rm calc}$ to vary rapidly with respect to the coordinates of the nitrogen and hydrogen atoms. The steep gradient in parameter space of F_{510} with incorrect sign is sufficient to offset the effect of the rest of the data.

(b) Second-order rigid-body refinement

The refinement was then repeated using the second-order theory (correct to $\langle\omega^2\rangle^2$) given in paper I. The variable parameters were the same as in the first-order refinement and are listed in column 3 of Table 4. The R index was 3·02%, which is a much smaller reduction than would be expected if the parameter $\langle\omega^2\rangle^2$ determined the third cumulants adequately (see § 6). In fact we would expect R to drop to about $3{\cdot}23\times 1{\cdot}18/2{\cdot}33 = 1{\cdot}64\%$.

6. Comparison of cumulant-expansion and rigid-body models

In comparing the results from the four refinement procedures described in §§ 4 and 5, it will be useful first to derive expressions relating the atomic parameters b_{ij}, c_{ijk} with the molecular parameters $\langle u^2\rangle$ and $\langle\omega^2\rangle$.

The fractional coordinates of the carbon atom are $u'\,0\,0$, where the origin of coordinates coincides with the centre of the molecule and with the centre of libration (see Fig. 1). Thus the atom is along [100] and the angle Θ between the radius vector **r** and the scattering vector **Q** (Fig. 2 of paper I) is given by

$$\left.\begin{aligned} Q^2\sin^2\Theta &= \frac{4\pi^2}{a_0^2}(h_2^2+h_3^2)\\ Q\cos\Theta &= \frac{2\pi}{a_0}h_1\,. \end{aligned}\right\} \qquad (4)$$

Substituting (4) into equation (3.2) of paper I and equating corresponding coefficients of h_1, h_2, h_3, h_1^2 ... *etc.* in this new equation and equation (3), we obtain the cumulant relations for the carbon atom listed in Table 6.

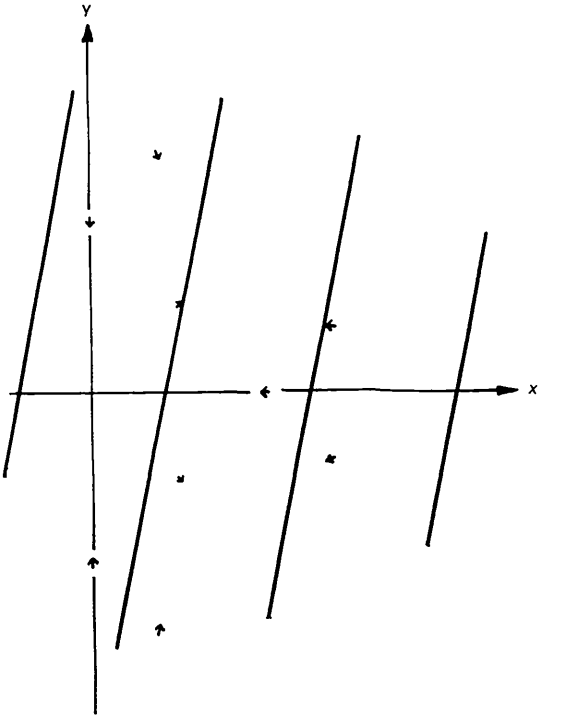

Fig. 5. Projection of the structure along [001]: the arrows start from the false minimum positions and end at the true minimum positions. The solid lines are zeros for the 510 reflexion.

The same procedure can be carried out for the nitrogen atom, where

$$Q^2 \sin^2 \Theta = \frac{4\pi^2}{a_0^2} \cdot \tfrac{2}{3} (h_1^2+h_2^2+h_3^2-h_1h_2-h_1h_3-h_2h_3)$$

$$Q \cos \Theta = \frac{2\pi}{a_0} \cdot \frac{1}{\sqrt{3}} (h_1+h_2+h_3) ,$$

and for the hydrogen atom, where

$$Q^2 \sin^2 \Theta = \frac{4\pi^2}{a_0^2} \cdot \frac{1}{2x^2+z^2} [h_1^2(x^2+z^2)+h_2^2(x^2+z^2) + 2h_3^2x^2-2h_1h_2x^2-2h_1h_3xz-2h_2h_3xz]$$

$$Q \cos \Theta = \frac{2\pi}{a_0} \cdot \frac{1}{(2x^2+z^2)^{1/2}} (h_1x+h_2x+h_3z) .$$

Table 7 lists the cumulant relations for nitrogen and Table 8 those for hydrogen. The three Tables 6–8

Table 5.

$h_1h_2h_3$	$F_{h_1h_2h_3}$										$F_{h_1k_2l_3}$	$h_1k_2l_3$
431	4·58	4·58	4·59	4·60	4·60	4·60	4·60	4·61	4·61	4·61	4·60	431
510	1·13	1·01	0·88	0·75	0·63	0·50	0·37	0·24	0·11	0·02	0·16	510
433	1·27	1·24	1·21	1·18	1·16	1·14	1·13	1·13	1·13	1·14	1·15	433
2,2,10	1·48	1·49	1·50	1·51	1·51	1·51	1·52	1·52	1·52	1·52	1·51	2,2,10
True minimum											False minimum	

Table 6. *Cumulant relations for carbon at* $(u'\ 0\ 0)$

Second cumulants	Third cumulants
$b_{11}=2\pi^2\left(\frac{\langle u^2\rangle}{a_0^2}+u'^2\langle\omega^2\rangle^2\right)$	$c_{122}=-\frac{4\pi^3}{3}u'^3\langle\omega^2\rangle^2$
$b_{22}=2\pi^2\left(\frac{\langle u^2\rangle}{a_0^2}+u'^2\langle\omega^2\rangle-\frac{17}{12}u'^2\langle\omega^2\rangle^2\right)$	$=c_{133}$
$=b_{33}$	$c_{111}=c_{222}=c_{333}$
$b_{12}=b_{13}=b_{23}=0$	$=c_{112}=c_{113}=c_{223}$
	$=c_{233}=c_{123}$
	$=0$

Table 7. *Cumulant relations for the nitrogen atom at* $(v\ v\ v)$

Second cumulants	Third cumulants
$b_{11}=2\pi^2\left[\frac{\langle u^2\rangle}{a_0^2}+2v^2\langle\omega^2\rangle-\frac{11}{6}v^2\langle\omega^2\rangle^2\right]$	$c_{111}=-8\pi^3v^3\langle\omega^2\rangle^2$
$=b_{22}=b_{33}$	$=c_{222}=c_{333}$
	$=-2c_{123}$
$b_{12}=2\pi^2[-v^2\langle\omega^2\rangle+\frac{29}{12}v^2\langle\omega^2\rangle^2]$	$c_{112}=c_{122}=c_{113}$
$=b_{23}=b_{31}$	$=c_{133}=c_{223}$
	$=c_{233}$
	$=0$

Table 8. *Cumulant relations for the hydrogen atom at* $(x\ x\ z)$

Second cumulants	Third cumulants
$b_{11}=2\pi^2\left[\frac{\langle u^2\rangle}{a_0^2}+(x^2+z^2)\,(\langle\omega^2\rangle\right.$	$c_{111}=-4\pi^3x(x^2+z^2)\,\langle\omega^2\rangle^2$
$\left.-\frac{17}{12}\langle\omega^2\rangle^2)+x^2\langle\omega^2\rangle^2\right]$	$=c_{222}$
	$c_{333}=-8\pi^3x^2z\langle\omega^2\rangle^2$
$=b_{22}$	$c_{112}=-\frac{4\pi^3}{3}x(z^2-x^2)\,\langle\omega^2\rangle^2$
$b_{33}=2\pi^2\left[\frac{\langle u^2\rangle}{a0_2}+2x^2(\langle\omega^2\rangle\right.$	$=c_{122}$
$\left.-\frac{17}{12}\langle\omega^2\rangle^2)+z^2\langle\omega^2\rangle^2\right]$	$c_{133}=-2c_{112}=c_{233}$
$b_{12}=2\pi^2[-x^2(\langle\omega^2\rangle-\frac{29}{12}\,\langle\omega^2\rangle^2)]$	$c_{113}=-4\pi^3/3\,z(z^2-x^2)\,\langle\omega^2\rangle^2$
$b_{13}=2\pi^2[-xz(\langle\omega^2\rangle-\frac{29}{12}\,\langle\omega^2\rangle^2)]$	$=c_{223}$
$=b_{23}$	$c_{123}=-\frac{1}{2}c_{333}$

show that the third cumulant coefficients are zero for the first-order rigid-body treatment ($\langle\omega^2\rangle^2=0$). Thus the first-order treatment is equivalent to the second-cumulant analysis with the rigid-body constraint, and the second-order treatment to the second- and third-cumulant analysis with the same constraint.

The point symmetries of the sites occupied by the three kinds of atom in HMT require that the relations given in Table 2 hold between the second- and third-cumulant coefficients. All these relations are included automatically in Tables 6–8: the additional relations in these Tables represent the restrictions imposed by the rigid-body assumption alone.

Table 3, column 3 gives the calculated values of the second and third cumulant coefficients, as derived using Tables 6–8 and the rigid-body parameters for the second-order theory given in Table 4, column 3. There is reasonably good agreement between the calculated second cumulant coefficients and the unconstrained coefficients in column 2 of Table 3. The agreement is much less satisfactory for the third cumulant coefficients, which tend to calculate lower than the unconstrained values. The neglect of the influence of the internal modes of vibration may be responsible for this failure of the rigid-body model.* Thus although the refinement proceeds more satisfactorily for the second-order rigid-body model than for the first-order model (see § 5), the best fit is given by the cumulant-expansion model with third cumulants.

The atomic coordinates for this cumulant-expansion model (Table 3, column 2) need a librational correction

$$1-\langle\omega^2\rangle+\tfrac{5}{12}\langle\omega^2\rangle^2$$

(see paper I, § 3). Using $\langle\omega^2\rangle=49{\cdot}0$ deg^2 the correction is 0·985, and the revised atomic coordinates are:

$$\left.\begin{array}{lll} \text{carbon} & u' = & 0{\cdot}2391\ (8) \\ \text{nitrogen} & v = & 0{\cdot}1243\ (4) \\ \text{hydrogen} & x = & 0{\cdot}0918\ (8) \\ & z = & -0{\cdot}3278\ (12)\,. \end{array}\right\} \qquad (5)$$

These give bond lengths, basd one $a_0=7{\cdot}019$ Å measured at 20 °C, of

$$\text{C–N}=1{\cdot}474\ \text{Å}$$
$$\text{and C–H}=1{\cdot}104\ \text{Å}\,,$$

representing what are possibly the most accurate bond lengths for C–N and C–H given by the diffraction method. The bond angles are: NCN = 113·7°, CNC = 107·3°, HCH = 111·3°, HCN = 108·0°.

7. Comparison of neutron and X-ray results: valence electron distribution

The X-ray data of Becka & Cruickshank (1963) have been analysed in combination with the present neutron measurements to examine whether there are any significant differences between the positions of the atoms determined by the two methods. Neutron diffraction yields the positions of the atomic nuclei whereas X-ray diffraction gives the positions of the centroids of the atomic charge clouds; these two positions will fail to coincide if the distribution of valence electrons is not centred on the atomic nuclei.

For HMT the following effects can be anticipated:

(i) Carbon. The valence electrons are in four orthogonal hybrid orbitals, giving a resulting charge-cloud which is symmetrical about the carbon nucleus. No difference is expected between neutron and X-ray positions.

(ii) Nitrogen. There are five electrons in the valence shell, again occupying orthogonal hybrid orbitals of *s* and *p*; three electrons participate in bonding and the remaining two are in lone-pair orbitals which are displaced from the nucleus in a direction away from the centre of the molecule. The net result is a displacement of the centroid of the charge cloud towards the lone-pair orbitals (Dawson, 1964). Calculations by Coulson (1970) indicate that the magnitude of this displacement is about 0·016 Å.

(iii) Hydrogen. As a result of bond formation, charge density builds up in the overlap region. Thus the CH length determined with X-rays is expected to be less than that given by neutrons.

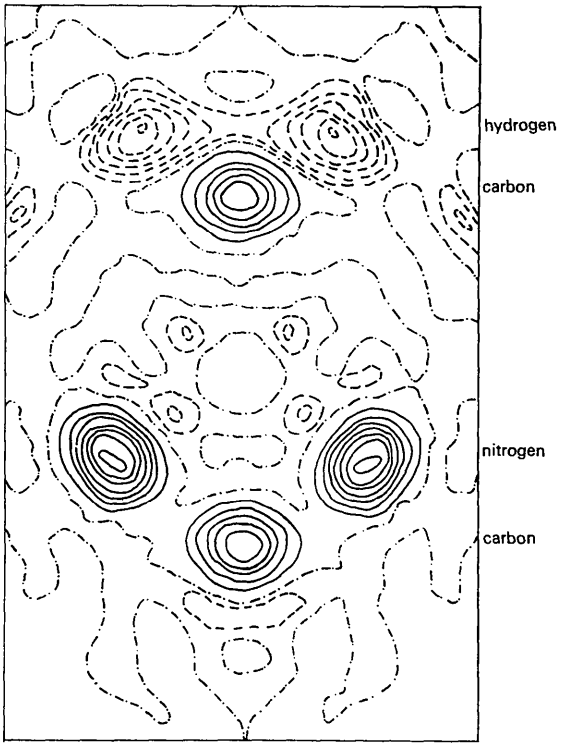

Fig.6. Neutron Fourier synthesis: (110) section through the centre of the molecule showing two hydrogen, two carbon and two nitrogen atoms.

† The contribution to the second and third cumulants caused by the internal modes is being investigated.

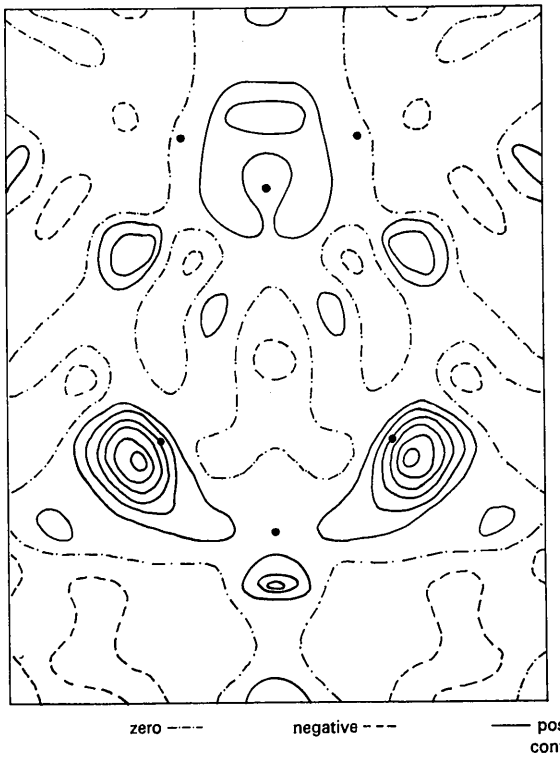

Fig.7. Difference Fourier synthesis, using X-ray structure-factor data and neutron positions. The peaks near the nitrogen atoms are due to the lone-pair electrons of nitrogen. The atomic nuclei are represented by dots.

All three expectations (i), (ii), (iii) are confirmed by the present study. (The numerical values of the neutron and X-ray parameters are tabulated in a separate paper by Duckworth, Willis & Pawley (1969), describing a new procedure for the joint analysis of neutron and X-ray diffraction data.) Thus the neutron and X-ray positions for the carbon atom are within one standard deviation of one another; the X-ray position for nitrogen is displaced by 0·018 Å from the neutron position and in a direction away from the molecular centre; and the CH bond obtained with X-rays is 0·04 Å shorter than that for neutrons.

The displacement of the charge centroid of the nitrogen atom is particularly striking, and is illustrated by the two electron density maps in Figs. 6 and 7. Fig. 6 is a (110) section through the centre of the molecule showing the nuclear density distribution calculated from the neutron data alone. The section includes all three kinds of atom, whose contours are slightly elongated because of the influence of librational motion about the inertial centre of the molecule. Fig. 7 is a difference Fourier synthesis for the same section with Fourier terms

$$(|F^X| - |F'|) \exp(i\varphi),$$

where $|F^X|$ is the observed X-ray structure factor of Becka & Cruickshank, $|F'|$ is the calculated X-ray structure factor and φ the calculated phase factor, the last two terms being derived using the neutron positions in equation (5). The difference Fourier synthesis clearly shows the presence of the lone-pair electrons associated with the nitrogen atom.

The authors are indebted to Dr Carroll K. Johnson for making available a least-squares program for third-cumulants refinement, and to Mr S. K. Sikka for assistance in the analysis.

References

ANDRESEN, A. F. (1957). *Acta Cryst.* **10**, 107.
ARNDT, U. W. & WILLIS, B. T. M. (1966). *Single Crystal Diffractometry*, p.297. Cambridge Univ. Press.
BECKA, L. N. & CRUICKSHANK, D. W. J. (1963). *Proc. Roy. Soc.* A **273**, 435.
BRILL, R., GRIMM, H. G., HERMANN, C. & PETERS, C. (1939). *Ann. Phys. Lpz.* **34**, 393.
COOPER, M. J. & ROUSE, K. D. (1968). *Acta Cryst.* A **24**, 405.
COULSON, C. A. (1970). *Thermal Neutron Diffraction*, Ch.5. Oxford Univ. Press.
DAWSON, B. (1964). *Acta Cryst.* **17**, 990.
DONOHUE, J. & GOODMAN, S. H. (1967). *Acta Cryst.* **22**, 352.
DUCKWORTH, J. K., WILLIS, B. T. M. & PAWLEY, G. S. (1969). *Acta Cryst.* A **25**, 482.
HAUSSÜHL, S. (1958). *Acta Cryst.* **11**, 58.
JOHNSON, C. K. (1970). *Thermal Neutron Diffraction*, Ch.9. Oxford Univ. Press.
LOBATCHEV, A. N. (1954). *Trav. Inst. Cristallogr. Moscow*, **10**, 172.
ROUSE, K. D. (1969). Private communication.
WILLIS, B. T. M. (1969). *Acta Cryst.* A **25**, 277.
WILLIS, B. T. M. & PAWLEY, G. S. (1970). *Acta Cryst.* A **26**, 254.
ZACHARIASEN, W. H. (1967). *Acta Cryst.* **23**, 558.